AIP | Applied Physics Letters

Mechanical 144GHz beam steering with all-metallic epsilon-near-zero lens antenna

V. Pacheco-Peña, V. Torres, B. Orazbayev, M. Beruete, M. Navarro-Cía, M. Sorolla, and N. Engheta

Citation: Applied Physics Letters **105**, 243503 (2014); doi: 10.1063/1.4903865
View online: http://dx.doi.org/10.1063/1.4903865
View Table of Contents: http://scitation.aip.org/content/aip/journal/apl/105/24?ver=pdfcov
Published by the AIP Publishing

Mechanical 144 GHz beam steering with all-metallic epsilon-near-zero lens antenna

V. Pacheco-Peña,[1,a)] V. Torres,[1,b)] B. Orazbayev,[1,c)] M. Beruete,[1,d)] M. Navarro-Cía,[2,3,4,e)] M. Sorolla,[1] and N. Engheta[5,f)]
[1]*Antennas Group-TERALAB, Universidad Pública de Navarra, Campus Arrosadía, 31006 Pamplona, Spain*
[2]*Optical and Semiconductor Devices Group, Department of Electrical and Electronic Engineering, Imperial College London, London SW7 2BT, United Kingdom*
[3]*Centre for Plasmonics and Metamaterials, Imperial College London, London SW7 2AZ, United Kingdom*
[4]*Centre for Terahertz Science and Engineering, Imperial College London, London SW7 2AZ, United Kingdom*
[5]*Department of Electrical and Systems Engineering, University of Pennsylvania, Philadelphia, Pennsylvania 19104, USA*

(Received 18 September 2014; accepted 28 November 2014; published online 15 December 2014)

An all-metallic steerable beam antenna composed of an ε-near-zero (ENZ) metamaterial lens is experimentally demonstrated at 144 GHz ($\lambda_0 = 2.083$ mm). The ENZ lens is realized by an array of narrow hollow rectangular waveguides working just near and above the cut-off of the TE_{10} mode. The lens focal arc on the xz-plane is initially estimated analytically as well as numerically and compared with experimental results demonstrating good agreement. Next, a flange-ended WR-6.5 waveguide is placed along the lens focal arc to evaluate the ENZ-lens antenna steerability. A gain scan loss below 3 dB is achieved for angles up to $\pm 15°$. © *2014 AIP Publishing LLC*.
[http://dx.doi.org/10.1063/1.4903865]

Within the framework of metamaterials,[1,2] artificial materials with ε-near-zero (ENZ) have been increasingly studied over the past few years due to their almost infinite phase velocity property providing interesting effects such as squeezing, tunneling, and supercoupling reported initially at microwaves.[3–7] These properties have also been demonstrated recently using metal-dielectric-metal multilayers at near infrared and visible frequencies.[8–10] However, a simple, yet effective approach to engineer ENZ-media for microwaves and the intermediate terahertz regime relies on exploiting the dispersive behavior of narrow hollow rectangular waveguides working near the cut-off frequency of the dominant mode TE_{10}.[5]

ENZ-media hold promise for different applications such as nanocircuits,[11] dielectric sensing,[12] multi-beam antennas,[13] and power splitting.[14] Nevertheless, it is in the field of lenses where they have been more intensively investigated.[15–18] Unlike other metamaterial lenses,[15,19–27] narrow hollow waveguides based ENZ lenses offer reduced reflection losses due to the squeezing/tunneling/supercoupling effect-induced impedance matching with free space.[16,17] In addition, ENZ-lenses realized by all-metallic narrow hollow rectangular waveguides have several advantages in comparison with lenses made partially or wholly from dielectrics, such as resistant to hazardous conditions and higher operation power. Moreover, given the concave profile of an ENZ-lens,[28] the illumination efficiency is improved compared with common dielectric lenses and some metamaterial lenses with convex profiles whose most distant edges are poorly illuminated.[22,29]

In this paper, the mechanical beam steering capabilities of an all-metallic plano-concave ENZ-lens antenna[16,18] are experimentally demonstrated at 144 GHz (D-band of millimeter waves). First, the radiated power is measured at seven different angles (0°, 3°, 6°, 9°, 12°, 15°, and 18°) as a function of the feeder position on the xz-plane. Owing to reciprocity, this is equivalent to raster scanning the xz-plane when the ENZ-lens is illuminated obliquely from its planar interface. These results are supported with analytical calculations based on the Huygens-Fresnel principle and numerical simulations using a plane-wave under the proper oblique incidence illumination. Second, the steering capability of the proposed ENZ-lens antenna is experimentally demonstrated by measuring the radiation pattern while shifting a flange-ended WR-6.5 waveguide used as a feeder at the experimental foci positions obtained in the first experiment. The experimental and analytical results demonstrate a high gain of 11 dB for 0° at the operational frequency and a gain scan loss below 3 dB for steering up to $\pm 15°$.

The fabricated plano-concave ENZ-lens is shown in Fig. 1(a). It is designed with an array of narrow hollow rectangular waveguides with a periodicity of $d_x \sim 1.4$ mm and $d_y = 0.5$ mm, along x and y axes, respectively. The hollow aperture of each single waveguide is $h_x = 1.1 \pm 0.025$ mm. With this dimension, the cut-off frequency of the dominant mode TE_{10} is 136.36 GHz. In order to achieve impedance matching with free space, a very small value of the dimension h_y must be chosen, with a magnitude of $h_y = h_x/42 = 0.05 \pm 0.02$ mm (i.e., $h_y \ll h_x$), see Ref. 18 for a detailed illustration of the unit cell. The whole lens is fabricated with total dimensions $L_x = 76.2$ mm, $L_y = 86.2$ mm, and $L_z = 40$ mm, with a total number of 33×144 narrow hollow waveguides along x- and y-axes, respectively. As it has

[a)]Electronic mail: victor.pacheco@unavarra.es
[b)]Electronic mail: victor.torres@unavarra.es
[c)]Electronic mail: b.orazbayev@unavarra.es
[d)]Electronic mail: miguel.beruete@unavarra.es
[e)]Electronic mail: m.navarro@imperial.ac.uk
[f)]Electronic mail: engheta@ee.upenn.edu

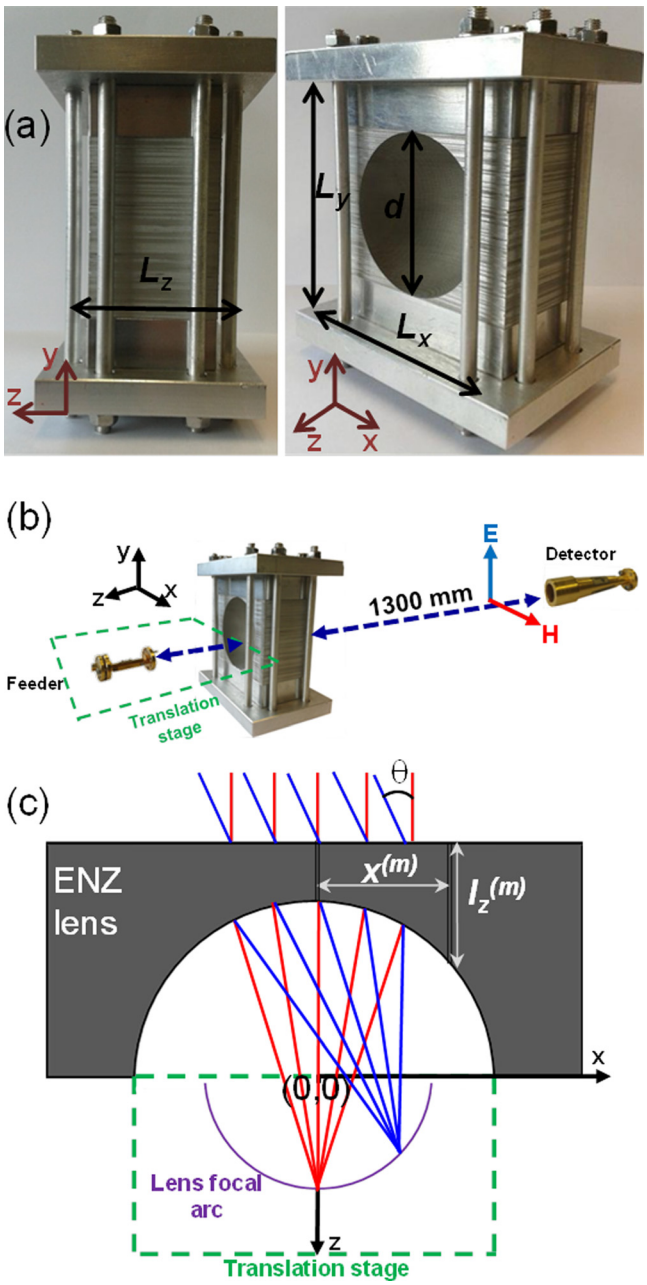

FIG. 1. (a) Lateral (left) and perspective (right) view of the fabricated ENZ-lens at the D-band of the millimeter waves with total dimensions: $L_x = 76.2$ mm, $L_y = 86.2$ mm, $L_z = 40$ mm, and $d = 55.5$ mm. (b) Experimental configuration used to characterize the radiation pattern of the lens. (c) Top view of the setup shown in (b) along with the lens focal arc (purple curve).

been described previously, metallic waveguides working near cut-off can emulate an ENZ medium with near zero values of propagation constant and phase advance inside the medium. Therefore, as it has been mentioned previously, if one face of the lens is planar, the other one should be designed with a concave hemi-spherical profile[15,28] instead of convex in order to convert a spherical phase front into a planar phase front or vice versa. This is because the EM waves emerging from an ENZ-medium are perpendicular to its surface.[6,14,16] In our case, the concave profiled face is designed with a diameter $d = 55.5$ mm.[18] Notice that the inner concave surface of the lens represents an ideal case for proper illumination by an antenna in comparison to convex lenses. The latter suffer from worse/lower illumination of the most distant edges of the lens as well as diffraction from them leading to undesirable side-lobes in the radiation pattern. The more effective illumination of the concave lenses yields to more homogeneous output phase fronts, and thus, higher antenna gain can be reached.

In order to evaluate the performance of the ENZ-lens under oblique incidence from the flat side of the lens, the equivalent effective isotropic 2D lens is studied analytically, applying the Huygens-Fresnel approximation considering an array of isotropic dipoles emitting cylindrical waves and placed at the output of each waveguide. Moreover, each dipole emits with unit amplitude and phase (ϕ) calculated as

$$\phi^{(m)} = k_0[\sqrt{\varepsilon_{r\_eff}}\, l_z^{(m)} + \sin(\theta) x^{(m)}], \tag{1}$$

where, $m = 0, 1, 2, 3, \ldots$, represents the waveguide number, $l_z^{(m)}$ is the length of the mth waveguide calculated as

$$l_z^{(m)} = \left(\frac{d}{2}\right) - \sqrt{\left(\frac{d}{2}\right)^2 - [x^{(m)}]^2},$$

$x^{(m)}$ is the position of each waveguide along x-axis [see Fig. 1(c)], k_0 is the wavenumber in free space calculated as $2\pi f/c$ with c the velocity of light in the medium filling the waveguide, θ is the angle of incidence of the plane-wave, and ε_{r_eff} is the effective permittivity of the lens. In our case, the experimental ENZ frequency is 144 GHz ($\lambda_0 = 2.083$ mm), which is above the cut-off frequency of the waveguides and is used as the operating frequency. At this frequency, the effective permittivity value of the ENZ lens is $\varepsilon_{r\_eff} = 0.103$.[18] Based on this, the analytical results of the normalized power distribution in the xz-plane (in front of the concave face of the lens) are shown in Figs. 2(a)–2(g) when a plane-wave impinges on the flat surface with the input angles: $\theta = 0°$, 3°, 6°, 9°, 12°, 15°, and 18°, respectively. It is clearly observed that the focal spot is deflected on the xz-plane when a plane wave impinges obliquely.

Moreover, in order to validate the analytical model and extend the theoretical analysis, the whole fabricated 3D lens was modeled using the finite-integration software CST Microwave Studio™. To this end, the transient solver was used along with an extremely fine hexahedral mesh with a minimum mesh size along x-axis of 0.0125 mm ($0.006\lambda_0$) and a total number of $\sim 370 \times 10^6$ mesh cells.

Aluminum ($\sigma_{Al} = 3.56 \times 10^7$ S/m) was chosen for the metallization and the lens was illuminated from its planar face with a vertically polarized (E_y) plane-wave varying the angle of incidence. Simulation results of the normalized power distribution on the xz-plane are presented in Figs. 2(h)–2(n) for the input angles $\theta = 0°$, 3°, 6°, 9°, 12°, 15,° and 18°, respectively. They confirm the deflection of focal spot in good agreement with the analytical calculations using Huygens-Fresnel approximation.

The experimental characterization was performed using an ABmm™ Millimeter-Wave Vector Network Analyzer [see schematic in Figs. 1(b) and 1(c)] and the procedure was as follows: The lens was rotated at the desired output angle (OA) ($\theta = 0°$, 3°, 6°, 9°, 12°, 15°, and 18°) with respect to the a D-band horn antenna placed at 1300 mm ($\sim 624\lambda_0$) from the planar face of the lens. After this, a 2D scan was

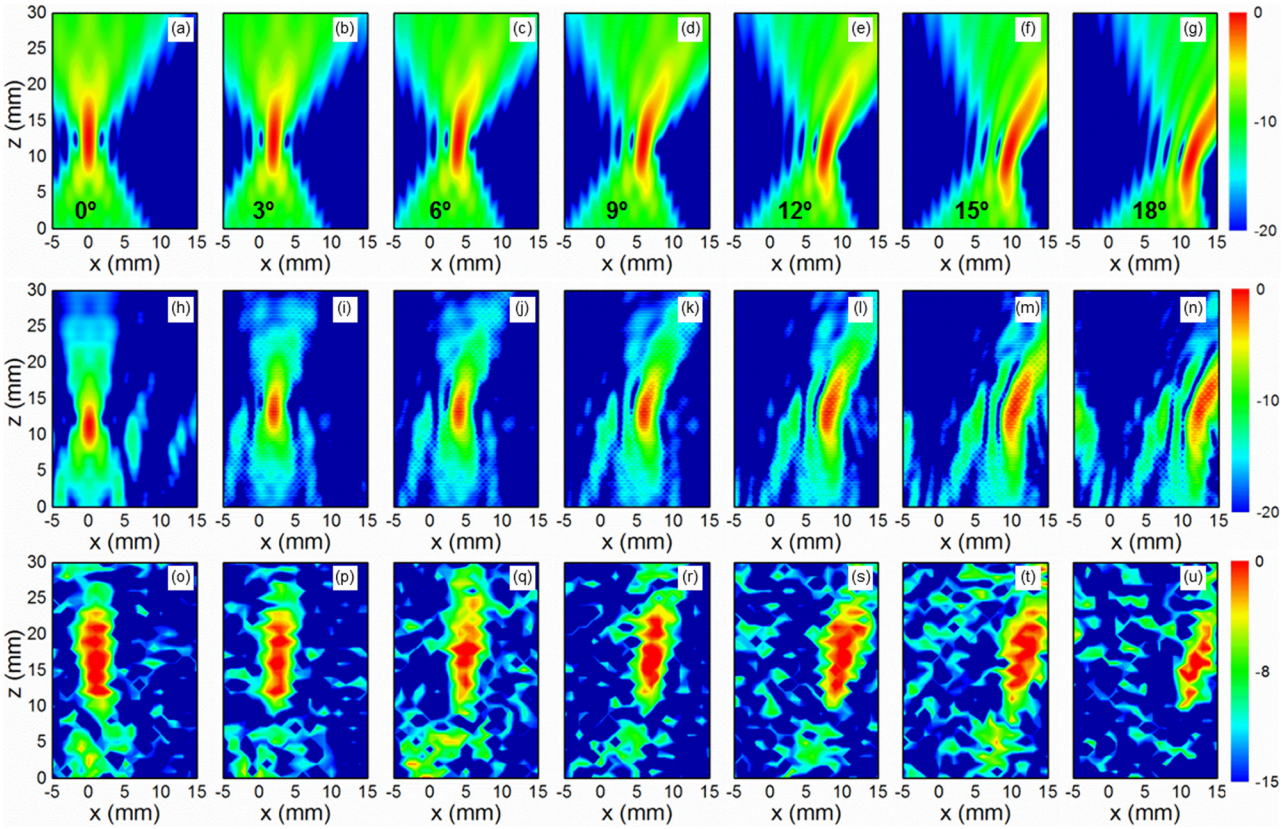

FIG. 2. Normalized spatial distribution of power on *xz*-plane for angles from 0° to 18° with a step of 3°: 2D analytical results using the Huygens-Fresnel approximation (a)–(g), 3D simulation results using the commercial software CST Microwave Studio™ (h)–(n) and experimental results (o)–(u). The scale bar is in dB.

performed on the *xz*-plane by moving a flange-ended WR-6.5 waveguide from −5 to 15 mm and from 0 to 30 mm along *x*- and *z*-axes respectively with a step of 1 mm. This was done for every illumination angle. This experiment allows us to reproduce the aforementioned simulation and thus to find experimentally the lens focal arc.

The experimental results of the normalized spatial power distribution on the *xz*-plane are presented in Figs. 2(o)–2(u) for the angles $\theta = 0°$, 3°, 6°, 9°, 12°, 15°, and 18°, respectively. By inspecting the whole Fig. 2, it is clear that the analytical, simulation and experimental results follow similar trends. For a quantitative comparison, the positions of the maximum (i.e., focus) on the *xz*-plane for each study are summarized in Table I. Note that for all the experimental cases, the positions along *x* are in good agreement with analytical and numerical results. However, there is some disagreement in the *z* position. This can arguably be due to the effect of the flange-ended WR-6.5 waveguide and its phase center uncertainty, which is not considered in the theoretical study. Finally, the maximum deflection experienced by the focus happens as expected for $\theta = 18°$ and is ($x = 11.5$, $z = 9.9$), ($x = 12.4$, $z = 12.8$), and ($x = 14.5$, $z = 16$) for the analytical, simulation, and experimental results, respectively.

TABLE I. Analytical, simulation, and experimental positions of the focus on the *xz*-plane. (All the values are in mm.)

Results	Coordinate	$\theta = 0°$	$\theta = 3°$	$\theta = 6°$	$\theta = 9°$	$\theta = 12$	$\theta = 15°$	$\theta = 18°$
Analytical	*x*	0	2	3.9	5.9	7.8	9.6	11.5
	z	12.3	12.3	11.9	11.7	11.2	10.4	9.9
Simulation	*x*	0	1.8	4	5.8	8	10.2	12.4
	z	11.6	13.2	13.2	13.2	13.2	13.2	12.8
Experimental	*x*	1	2	4	6	10	11	14.5
	z	17	17	18	16	16	15	16

Once the experimental lens focal arc was found, the flange-ended rectangular waveguide was placed at each position of Table I, and the angular distribution of the lens antenna radiation from the planar side was measured for −25° to 10° with a step of 0.5°. Experimental results of the normalized radiation pattern are presented in the left column of Fig. 3 (each curve is normalized to the maximum obtained at 0°). Moreover, by using the Huygens-Fresnel approximation, the power angular distribution at the same distance as for experimental measurements (1300 mm ∼ $624\lambda_0$) is calculated for each OA and shown in the right column of Fig. 3. It can be observed that both, analytical and experimental, results are in good agreement with the experimental OA's close to the values calculated analytically.

The analytical and experimental results of the beam steering performance of the ENZ-lens are compared quantitatively in Table II in terms of the OA, maximum normalized radiation power (MNRP) at the OA, half power beam width (θ_{-3dB}), and side lobe level (SLL). It can be observed that the OA's are close to the original angle. Moreover, it is shown that the experimental values of the θ_{-3dB} are between 2.5° and 4.5° with the minimum for the OA of 0° and maximum for the higher angle (18°) as expected. It can be observed that the same analytical θ_{-3dB} is obtained for all

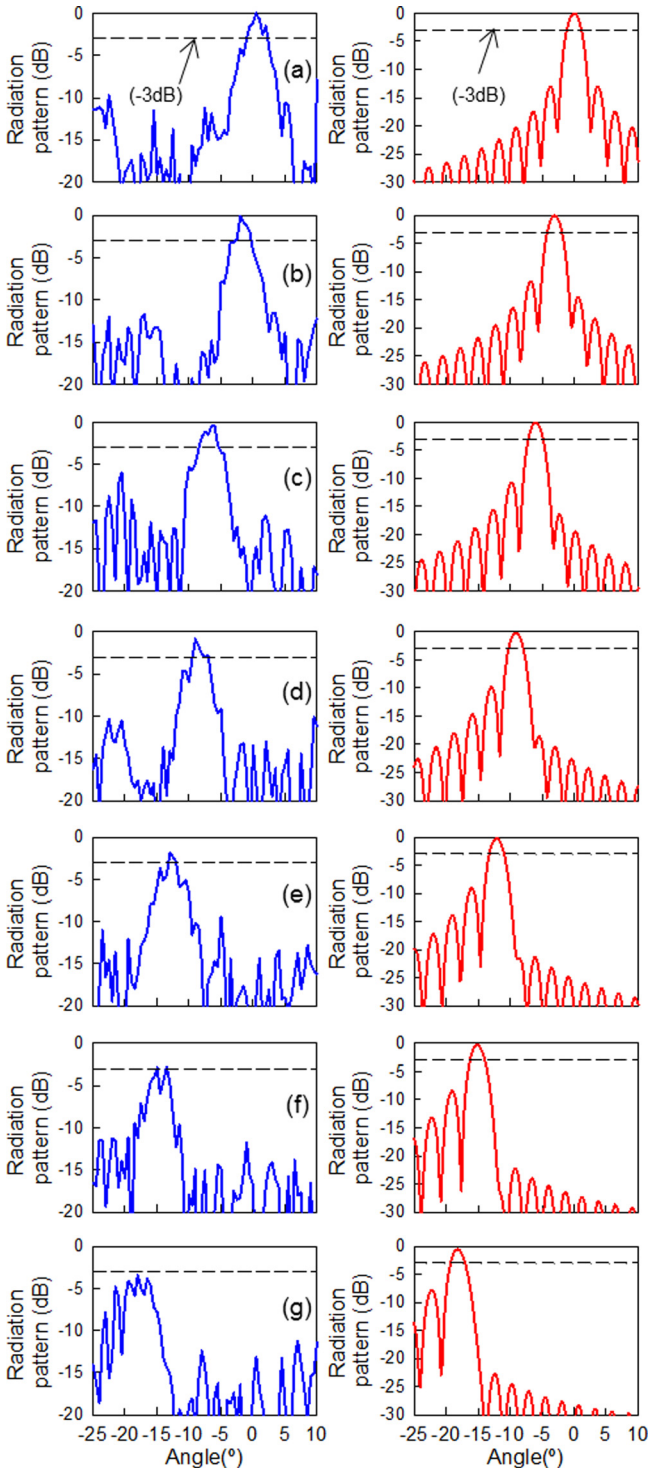

FIG. 3. Experimental (left column) and 2D analytical (right column) of the normalized radiation pattern for the output angles: (a) 0°, (b) 3°, (c) 6°, (d) 9°, (e) 12°, (f) 15°, and (g) 18° when the feeder is placed at the experimental and analytical (x,z) coordinates of Table I, respectively. The black dashed line on each plot corresponds to −3 dB, which is a standard of the maximum scan loss allowed for a suitable beam steering.

the OA's because of the ideal conditions. Furthermore, the higher side lobe level is obtained for an OA of 18° in the experiment with a value of −4.85 dB, which is closer to the main lobe compared with the other angles. The experimental gain (defined as the ratio of the radiated power density in the direction of maximum emission and the power density radiated by an ideal lossless isotropic radiation that emits all the power fed by the source[26]) at the working frequency (144 GHz) has a maximum of 11 dB at 0°, which is obtained comparing the ENZ-lens with a horn antenna using the comparison method.[30] Moreover, it is shown that the maximum normalized radiation power at 18° is below −3 dB, which is used as a standard of the maximum scan loss allowed for a suitable beam steering. Based on this, the ENZ-lens here proposed has a suitable beam steering up to ±15°.

TABLE II. Experimental and analytical results of the beam steering performance using the ENZ-lens.

OA[a] (°)			MNRP[b] (dB)		θ_{-3dB}[c] (°)		SLL[d] (dB)	
Original	Exp.	Analytical	Exp.	Analytical	Exp.	Analytical	Exp.	Analytical
0	0.5	0	0	0	2.5	2.2	−10.57	−12.8
3	2	3	−0.05	−0.093	3.75	2.2	−11.58	−11.45
6	6	6	−0.36	−0.06	4	2.2	−5.3	−10.9
9	9	9.2	−0.84	−0.37	3	2.2	−10.5	−10
12	13	12.2	−1.88	−0.57	3	2.2	−9.5	−9.81
15	15	15	−2.87	−0.78	2.5	2.2	−11.3	−8.52
18	18	18	−3.45	−1.29	4.5	2.2	−4.85	−7.65

[a]OA is the output angle.
[b]MNRP is the maximum normalized radiation power at the output angle.
[c]θ_{-3dB} is the half power beam width.
[d]SLL is the side lobe level.

In conclusion, the mechanical beam steering performance of a plano-concave ENZ-lens working at the D-band of millimeter waves has been demonstrated experimentally and compared with 3D full-wave numerical simulations and 2D analytical results using the Huygens-Fresnel approximation. By invoking reciprocity, the experimental lens focal arc is found, which is in good agreement with numerical and analytical results. The beam steering capability of the ENZ-lens has been experimentally studied by placing the feeder at the focal positions along the lens focal arc obtained experimentally and evaluating the radiation pattern. A high gain of 11 dB at 144 GHz has been experimentally obtained at 0°. Meanwhile, the gain scan loss (figure of merit used to evaluate the steering performance of a lens antenna) remains below 3 dB up to ±15°. The lens here presented may find applications in antenna's systems that require steerable performance of the output beam with high gain and low losses under hazardous conditions.

This work was supported in part by the Spanish Government under Contract Consolider Engineering Metamaterials CSD2008-00066 and Contract TEC2011-28664-C02-01. V.P.-P. is sponsored by Spanish Ministerio de Educación, Cultura y Deporte under grant FPU AP-2012-3796. V.T. is sponsored by the Universidad Pública de Navarra. B.O. is sponsored by Spanish Ministerio de Economía y Competitividad under Grant FPI BES-2012-054909. M.B. is sponsored by the Spanish Government via RYC-2011-08221. M.N.-C. is supported by the Imperial College Junior Research Fellowship. The authors are in debt to the technology center Tekniker for the precise fabrication of the lens. In memoriam of our beloved friend Mario Sorolla.

[1]N. Engheta and R. Ziolkowski, *Metamaterials: Physics and Engineering Explorations*, 1st ed. (John Wiley & Sons/IEEE Press, USA, 2006), p. 440.
[2]L. Solymar and E. Shamonina, *Waves in Metamaterials* (Oxford University Press, New York, 2009).
[3]M. Silveirinha and N. Engheta, Phys. Rev. Lett. **97**, 157403 (2006).
[4]M. G. Silveirinha and N. Engheta, Phys. Rev. B **76**, 245109 (2007).
[5]B. Edwards, A. Alù, M. Young, M. Silveirinha, and N. Engheta, Phys. Rev. Lett. **100**, 033903 (2008).
[6]A. Alù, M. Silveirinha, A. Salandrino, and N. Engheta, Phys. Rev. B **75**, 155410 (2007).
[7]A. Alù, M. G. Silveirinha, and N. Engheta, Phys. Rev. E **78**, 016604 (2008).
[8]G. Subramania, A. J. Fischer, and T. S. Luk, Appl. Phys. Lett. **101**, 241107 (2012).
[9]R. Maas, J. Parsons, N. Engheta, and A. Polman, Nat. Photonics **7**, 907 (2013).
[10]J. Gao, L. Sun, H. Deng, C. J. Mathai, S. Gangopadhyay, and X. Yang, Appl. Phys. Lett. **103**, 051111 (2013).
[11]N. Engheta, Science **317**, 1698 (2007).
[12]A. Alù and N. Engheta, Phys. Rev. B **78**, 045102 (2008).
[13]J. Yang, M. Huang, J. Peng, and Z. Xiao, AEU—Int. J. Electron. Commun. **65**, 543 (2011).
[14]V. Pacheco-Peña, V. Torres, M. Beruete, M. Navarro-Cía, and N. Engheta, J. Opt. **16**, 094009 (2014).
[15]M. Navarro-Cía, M. Beruete, I. Campillo, and M. Sorolla, Phys. Rev. B **83**, 115112 (2011).
[16]M. Navarro-Cía, M. Beruete, M. Sorolla, and N. Engheta, Phys. Rev. B **86**, 165130 (2012).
[17]V. Torres, V. Pacheco-Peña, P. Rodríguez-Ulibarri, M. Navarro-Cía, M. Beruete, M. Sorolla, and N. Engheta, Opt. Express **21**, 9156 (2013).
[18]V. Torres, B. Orazbayev, V. Pacheco-Peña, J. Teniente, M. Beruete, M. Navarro-Cia, M. Sorolla, and N. Engheta, "Experimental demonstration of a millimeter-wave metallic ENZ lens based on the energy squeezing principle," IEEE Trans. Antennas Propag. (published online).
[19]P. Alitalo, O. Luukkonen, J. Vehmas, and S. A. Tretyakov, IEEE Antennas Wireless Propag. Lett. **7**, 187 (2008).
[20]M. Beruete, M. Navarro-Cía, M. Sorolla, and I. Campillo, Opt. Express **16**, 9677 (2008).
[21]M. Navarro-Cía, M. Beruete, M. Sorolla, and I. Campillo, Appl. Phys. Lett. **94**, 144107 (2009).
[22]A. Demetriadou and Y. Hao, IEEE Antennas Wireless Propag. Lett. **10**, 1590 (2011).
[23]T. Zentgraf, Y. Liu, M. H. Mikkelsen, J. Valentine, and X. Zhang, Nat. Nanotechnol. **6**, 151 (2011).
[24]D.-H. Kwon and D. H. Werner, IEEE Antennas Wireless Propag. Lett. **8**, 1115 (2009).
[25]V. Pacheco-Peña, B. Orazbayev, V. Torres, M. Beruete, and M. Navarro-Cía, Appl. Phys. Lett. **103**, 183507 (2013).
[26]V. Pacheco-Peña, B. Orazbayev, U. Beaskoetxea, M. Beruete, and M. Navarro-Cía, J. Appl. Phys. **115**, 124902 (2014).
[27]J. Neu, B. Krolla, O. Paul, B. Reinhard, R. Beigang, and M. Rahm, Opt. Express **18**, 27748 (2010).
[28]M. Navarro-Cía, M. Beruete, I. Campillo, and M. Sorolla, IEEE Trans. Antennas Propag. **59**, 2141 (2011).
[29]A. Demetriadou and Y. Hao, Opt. Express **19**, 19925 (2011).
[30]IEEE Standard Test Procedures for Antennas, ANSI/IEEE Standard 149–1979, 1979.